Optical Spectra of Supernovae

David Branch[1], E. Baron[1], and David J. Jeffery[2]

[1] University of Oklahoma, Norman, OK 73019, USA
[2] New Mexico Institute of Mining and Technology, Socorro, NM 87801, USA

Abstract. Supernova flux and polarization spectra bring vital information on the geometry, physical conditions, and composition structure of the ejected matter. For some supernovae the circumstellar matter is also probed by the observed spectra. Some of this information can be inferred directly from the observed line profiles and fluxes, but because of the Doppler broadening and severe line blending, interpretation often involves the use of synthetic spectra. The emphasis in this Chapter is on recent results obtained with the help of synthetic spectra.

1 Introduction

As discussed and illustrated by M. Turatto in Chap. 3, optical spectra serve as the basis for the classification of supernovae (SNe). This chapter is concerned with extracting information from optical spectra on the geometry, physical conditions, and composition structure (element composition versus ejection velocity) of the ejected matter, and also the circumstellar matter for some SNe. Several other chapters of this volume also discuss certain aspects of SN spectroscopy: ultraviolet spectra (Chap. 7 by N. Panagia); the circumstellar and nebular spectra of SN 1987A (Chap. 15 by R. McCray); and the hypernova SN 1998bw (Chap. 25 by K. Iwamoto et al.).

Some of the information carried by SN spectra can be inferred directly from the observed line profiles and fluxes, but because SN ejection velocities are a few percent of the speed of light, spectral features generally are blended and interpretation often involves comparing observed spectra with synthetic spectra calculated for model SNe. The spectrum calculations may be simplified and rapid, or physically self-consistent and computationally intensive. Similarly, both simple parameterized physical models and numerical hydrodynamical models are used. In this chapter we place some emphasis on recent results obtained with the help of synthetic spectra.

In §2 the elements of spectral line formation in SNe are discussed and some of the synthetic spectrum codes that are in current use are described. In §§3–6 recent comparisons of synthetic spectra with observed spectra of SNe of Types Ia, Ib, Ic, and II are surveyed. Space limitations prevent us from referring to the numerous papers that have been important to the development of this subject; many such can be found in 1993 and 1997 review articles [134,36]. Here most of the references are to, and all of the figures are from, papers that have appeared since 1998. A brief discussion of the prospects for the future appears in §7.

2 Line Formation and Synthetic Spectrum Codes

At the time of the supernova explosion, physical scales are relatively small. Shortly thereafter the ejected matter expands freely as from a point explosion with each matter element having a constant velocity. All structures in the ejecta then just scale linearly with t, the time since explosion. The matter is in homologous expansion, which has several convenient features: (1) the radial velocity v of a matter element is a useful comoving coordinate with actual radial position of the element given by $r = vt$; (2) the density at any comoving point just scales as t^{-3}; (3) the photon redshift between matter elements separated by velocity Δv, $\Delta\lambda = \lambda(\Delta v/c)$, is time-independent; and (4) the resonance surfaces for line emission at a single Doppler-shifted line frequency are just planes perpendicular to the observer's line of sight. (Relativistic effects introduce a slight curvature [64].)

If continuous opacity in the line forming region is disregarded, the profile of an unblended line can be calculated when the line optical depth $\tau_\ell(v)$ and source function $S_\ell(v)$ are specified. Because SN ejection velocities ($\sim 10,000$ km s^{-1}) are much larger than the random thermal velocities (~ 10 km s^{-1}), a photon remains in resonance with an atomic transition only within a small resonance region. The Sobolev approximation, that the physical conditions other than the velocity are uniform within the resonance region, usually is a good one, and it allows the optical depth of a line to be simply expressed in terms of the local number densities of atoms or ions in the lower and upper levels of the transition:

$$\tau_\ell = \frac{\pi e^2}{m_e c}\ f\ \lambda\ t\ n_\ell \left(1 - \frac{g_\ell n_u}{g_u n_\ell}\right) = 0.229\ f\ \lambda_\mu\ t_d\ n_\ell \left(1 - \frac{g_\ell n_u}{g_u n_\ell}\right),$$

where f is the oscillator strength, λ_μ is the line wavelength in microns, t_d is the time since explosion in days, and n_ℓ and n_u are the populations of the lower and upper levels of the transition in cm^{-3}. The term in brackets is the correction for stimulated emission. The source function is

$$S_\ell = \frac{2hc}{\lambda^3}\ \left(\frac{g_u n_\ell}{g_\ell n_u} - 1\right)^{-1}.$$

All of the radial dependence of τ_ℓ and S_ℓ is in the level populations. The specific intensity that emerges from a resonance region is

$$I = S_\ell \left(1 - e^{-\tau_\ell}\right).$$

Spectroscopic evolution can be divided into a photospheric phase when the SN is optically thick in the continuum below a photospheric velocity, and a subsequent nebular phase during which the whole SN is optically thin in the continuum. In the photospheric phase line formation occurs above the photosphere and in the nebular phase throughout the ejecta. There is, of course, no sharp division between the two phases. However, spectral synthesis modeling techniques in the

photospheric and nebular limits can make use of different approximations which are adequate for those limits.

In the remainder of this section we first discuss line formation and synthetic spectrum codes in the photospheric and nebular phases under the assumptions of spherical symmetry and negligible circumstellar interaction. We then consider the effects of circumstellar interaction, and SN asymmetry and polarization spectra.

2.1 The Photospheric Phase

The elements of spectrum formation in the photospheric phase have been discussed and illustrated at length elsewhere [66]. Here we will only briefly summarize those elements and then discuss spectrum synthesis codes.

During the photospheric phase a continuum radiation field is emitted by a photosphere which can be idealized as an infinitely thin layer. Above the photosphere the radiation interaction with continuous opacity is small. Line opacity on the other hand can be very large for the strongest lines. The large Doppler shifts spread line opacity over a large wavelength interval increasing the effect of strong lines compared to a static atmosphere where such strong lines saturate and can only affect radiation in a narrow wavelength interval. The cumulative effect of many lines, strong and weak, can create a quasi-continuous opacity in the Eulerian frame. This effect has been called the "expansion opacity" [68,107]; it dominates in the ultraviolet, where it effectively pushes the photosphere out to a larger radius than in the optical. Full, co-moving, line-blanketed calculations automatically account for this effect [3]; introducing the observer's frame expansion opacity into comoving frame calculations is incorrect.

In the optical, which is usually the chief focus of analysis, the spectrum is characterized by P Cygni lines superimposed on the photospheric continuum. The P Cygni profile has an emission peak near the rest wavelength of the line and a blueshifted absorption feature. The peak may be formed in part by true emission or by line scattering into the line of sight of photons emitted by the photosphere. The emission peak would tend to be symmetrical about the line center wavelength if not for the blueshifted absorption. The absorption is formed by scattering out of the line of sight of photospheric photons emitted toward the observer. Since this occurs in front of the photosphere, the absorption is blueshifted. At early times the ejecta density is high, the photosphere is at high velocity, and the line opacity is strong out to still higher velocities. As expansion proceeds, the photosphere and the region of line formation recede deeper into the ejecta. The P Cygni line profile width thus decreases with time. The minimum of the absorption feature of weak lines tends to form near the photospheric velocity, thus weak lines (e.g., weak Fe II lines) can be used to determine the photospheric velocity's time evolution. The recession of the photosphere exposes the inner ejecta and permits its analysis.

In understanding P Cygni line formation in SNe it is conceptually useful, and often in simple parameterized radiative transfer modeling a good physical approximation, to consider the line-photon interaction as being pure resonance

scattering; i.e., no photon creation or destruction above the photosphere. Then the source function of an unblended line is just $S_\ell(v) = W(v)I_{\rm phot}$, where $W(v)$ is the usual geometrical dilution factor [99] and $I_{\rm phot}$ is the continuum specific intensity (assumed angle-independent) radiated by the photosphere. Given the pure resonance scattering approximation for an unblended P Cygni line, the emission is formed just by scattering into the line of sight and the absorption just by scattering out of the line of sight.

Unfortunately, in general there is strong line blending. A photon that is scattered by one transition can redshift into resonance with another, so the influence of each transition on others of longer wavelength must be taken into account. This multiple scattering corresponds to the observer's line blending. Calculations show that in blends, absorptions trump emissions: i.e., when resolved, the absorption minima of blends tend to be blueshifted by their usual amounts, but the emission peaks do not necessarily correspond to the rest wavelengths of the lines of the blend. Thus absorption minima usually are more useful than emission peaks for making line identifications during the photospheric phase.

If one has made the resonance scattering approximation for simple modeling, it turns out that the effect of line blending on source functions for some lines is often effectively very small. From a conceptual point of view it is convenient to think of $S_\ell(v) = W(v)I_{\rm phot}$ even for strongly blended lines. In general the effect of line blending on the emergent spectrum is significant and cannot be neglected.

A special case of a P Cygni line that has become of interest is a "detached" line: i.e, a line that has a significant optical depth only above some detachment velocity that exceeds the velocity at the photosphere. A detached line consists of a flat inconspicuous emission peak and an absorption having a sharp red edge at the blueshift corresponding to the detachment velocity (Fig 1). We shall later refer to the concept of detached lines in discussing particular observed spectra.

It is possible to extract some information from spectra by simple direct analysis. Recently a method for inverting an unblended P Cygni line profile to extract the radial dependences of the line optical depth and the source function has been developed [69]. But the complex blending of P Cygni lines (which often occurs), and the need to account for effects that cannot treated by direct approaches make analysis by synthetic spectrum modeling essential. Rather than discuss modeling in general we will briefly describe three synthetic spectrum codes that are frequently used, proceeding from simple to complex. Example synthetic spectra from these codes will appear in §§3 – 6.

The simplest code is the fast, parameterized `SYNOW` code. Technical details of the current version are in [38]. The basic assumptions are: spherical symmetry; a sharp photosphere that emits a blackbody continuous spectrum; and the Sobolev approximation with a resonance scattering source function. `SYNOW` does not do continuum transport, it does not solve rate equations, and it does not calculate or assume ionization ratios. Its main function is to take line multiple scattering into account so that it can be used in an empirical spirit to make line identifications and determine the velocity at the photosphere and the velocity intervals within which the presence of each ion is detected. For each ion that is introduced,

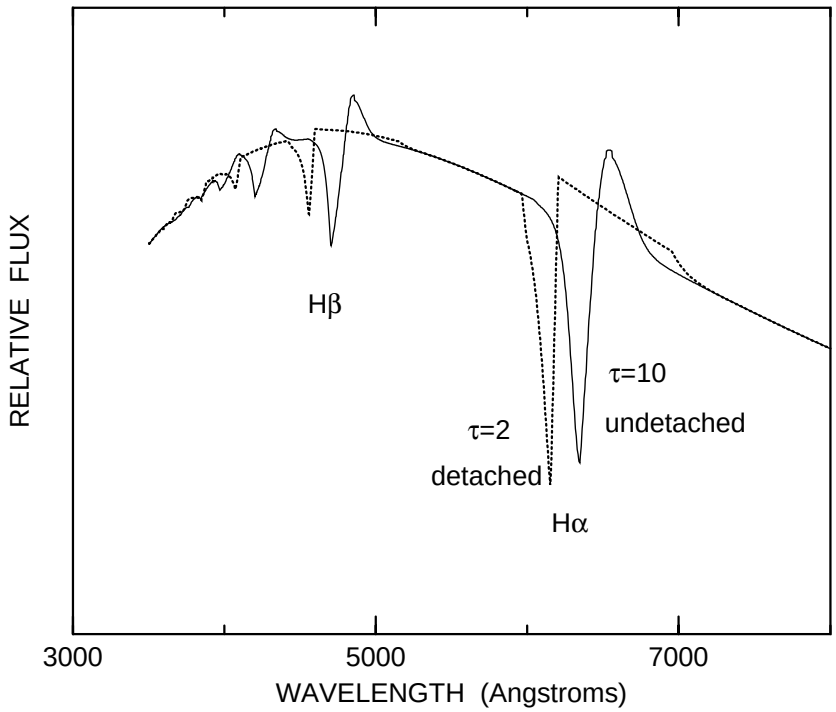

Fig. 1. A SYNOW synthetic spectrum (*dotted line*) that has $v_{phot} = 10,000$ km s^{-1} and hydrogen lines detached at 20,000 km s^{-1} where τ(Hα)=2, is compared with a synthetic spectrum (*solid line*) that has $v_{phot} = 10,000$ km s^{-1} and undetached hydrogen lines with τ(Hα) = 10 at the photosphere. (From [13])

the optical depth at the photosphere of a reference line is a free parameter, and the optical depths of the other lines of the ion are calculated assuming Boltzmann excitation. Reference lines are generally chosen as the strongest line in the optical for a particular species. Line optical depths are assumed to decrease radially following a power law or an exponential. When deciding which ions to introduce, use is made of the results of [50] who presented plots of LTE Sobolev line optical depths versus temperature for six different compositions that might be expected to be encountered in SNe, and sample SYNOW optical spectra for 45 individual ions that are candidates for producing identifiable spectral features in SNe. When fitting to an observed spectrum, the important parameters are the reference line optical depths, the velocity at the photosphere, and whatever maximum and minimum (detachment) velocities may be imposed on each ion.

Somewhat more complex synthetic spectrum calculations are carried out with what we will refer to as the ML MONTE CARLO code (ML for Mazzali and Lucy), technical details of which are in [91] and references therein. This code also assumes a sharp photosphere, makes the Sobolev approximation, and does not

solve rate equations. The main differences from SYNOW are: (1) an approximate radiative equilibrium temperature distribution and internally consistent ionization ratios are calculated for an assumed composition structure; (2) electron scattering in the atmosphere is taken into account; and (3) the original assumption of resonance scattering has been replaced by an approximate treatment of photon branching, to allow an absorption in one transition to be followed by emission in another [85]. Several circumstances in which the effects of photon branching are significant are discussed in [91].

Very detailed calculations are made with the multi-purpose synthetic spectrum and model atmosphere code called PHOENIX. Technical details of PHOENIX are in [53] (see also [6]). The basic assumptions are spherical symmetry and time independence. The Sobolev approximation is dispensed with, and calculations are carried out in the comoving frame with all special relativistic effects. The aim of PHOENIX is to take all of the relevant physics into account as fully as possible. PHOENIX treats continuum transport, solves the NLTE rate equations for a large number of ions and a very large number of atomic levels with gamma ray deposition and nonthermal excitation taken into account, and determines a self-consistent radiative equilibrium temperature structure. The lower boundary condition can be chosen to be either diffusive or nebular.

One may ask why simpler codes are needed when PHOENIX-like codes can be implemented. PHOENIX–like codes demand many hours of computation and are not optimal for explorations of parameter space or for gaining insight into how simple features of modeling affect outcomes. The simpler codes are tools for rapid exploration and gaining insight. Such codes, however, cannot give definitive determinations because of their simplified physics. PHOENIX–like calculations must be the basis for ultimate decisions about the viability of SN models.

2.2 The Nebular Phase

Our discussion of line formation in the nebular phase will be brief since the subject is discussed in Chap. 15, in the context of SN 1987A. (See also [41].)

In the absence of circumstellar interaction, the nebular phase is powered by radioactive decay, primarily ^{56}Co (77.23 day half-life), the daughter of explosion-synthesized ^{56}Ni (6.075 day half-life). At very late times longer lived radioactive species such as ^{57}Co and ^{44}Ti become important.

The decay gamma rays deposit their energy by Compton scattering off electrons to produce nonthermal fast electrons whose energy quickly goes into atomic ionization and excitation, and Coulomb heating of the thermal electrons [120]. Particularly for low mass SNe (Types Ia,b,c) the unscattered escape of gamma rays (which increases as the ejecta thins) causes the kinetic energy of positrons from the ^{56}Co decays to become an important energy source: about 3 % of the ^{56}Co decay energy is in the form of positron kinetic energy. The positrons are much more strongly trapped than the gamma rays—but not completely trapped [101]. The positron kinetic energy goes into creating fast electrons leading to the same deposition processes as the gamma rays. Optical emission lines are formed by

recombination, collisional excitation, and fluorescence. P Cygni profiles of permitted lines that form by scattering in the outer layers may be superimposed on the emission line spectrum.

Because of low continuous opacity and increasingly low line opacities, photons emitted by true emission processes are increasingly unlikely to be scattered again. Thus non-local radiative transfer effects in the nebular phase tend to become negligible. (Local trapping in an optical thick line can be treated easily using a Sobolev escape probability.) Thus (absent circumstellar interaction) it is somewhat more feasible than in the photospheric phase to extract information without making synthetic spectrum calculations. This was especially true of SN 1987A, which because of its proximity was well observed in the optical and the infrared long into the nebular phase when the characteristic velocity of the line forming region was only ~ 3000 km s^{-1} and blending was not too severe (see Chap. 15). Most other non-circumstellar interacting SNe are observed only for a year or so after explosion and line blending is more of a problem.

Without a photosphere, there is no continuum flux to be scattered out of the line of sight even if there are optically thick lines. Hence the characteristic line profile of the nebular phase is not a P Cygni profile, but an emission line that peaks near the rest wavelength and for several reasons may have an extended red wing [43,20]. If the line has significant optical depth down to low velocity, the emission line has a rounded peak. If instead the line forms in a shell, the emission has a boxy (flat top) shape with the half width of the box corresponding to the minimum velocity of the shell.

As for the photospheric phase, nebular-phase synthetic spectrum calculations of various levels of complexity prove to be useful. Relatively simple parameterized approaches that can be used as diagnostic tools are described by [10,42]. A one-zone code that was developed in its original form by [110] and will be referred to here as the `RL NEBULAR` code (RL for Ruiz-Lapuente and Lucy) is frequently used (e.g. [92,93,109]). The input parameters are the time since explosion and the mass, composition, and outer velocity of the nebula. Heating is calculated from the ^{56}Co decay rate, and cooling is by radiative emission. The electron density, temperature, NLTE level populations and emission line fluxes are determined simultaneously by enforcing statistical and thermal equilibrium. Codes for calculating synthetic spectra of hydrodynamical models are described by [60] and [83] and references therein. These multi-zone codes calculate the nonthermal heating, ionization equilibrium, and the NLTE level populations for a large number of atomic levels. Synthetic spectra of the CO molecule have also been calculated [32,45,118]. For a description of additional nebular phase codes that have been used for SN 1987A, see Chap. 15.

The photospheric phase forbids a direct view into the inner regions of the ejecta. The nebular phase permits this direct view, but, on the other hand, the outer layers tend toward invisibility. The photospheric phase demands a powerful radiative transfer technique. The advanced nebular phase requires almost none at all, at least in the optical; the ionizing photons in the UV may need a detailed radiative transfer treatment and, of course, the gamma ray and positron energy

depositions need a non-local transfer treatment probably best done by Monte Carlo. Both phases require NLTE treatments and extensive atomic data. The two phases offer complementary insights and challenges for analysis.

2.3 Circumstellar Interaction

The physics of the radiative and hydrodynamical interactions between SNe and their circumstellar matter (circumstellar interaction: CSI) are discussed in Chap. 14 by R.A. Chevalier & C. Fransson. No convincing detection of SN Ia CSI has yet been made in any wavelength band. CSI also does not seem to affect the optical spectra of typical SNe Ib, SNe Ic (but for an exception see [87]), and many SNe II. Some SNe II and perhaps some hyperenergetic SNe Ic are affected, and in extreme cases dominated, by CSI effects.

In the idealized case, the wind of the SN progenitor star has a constant velocity and a constant mass loss rate, and therefore an r^{-2} density distribution. After the explosion, the circumstellar matter can be heated and accelerated by the photons emitted by the SN. Subsequent hydrodynamic interaction between high velocity SN ejecta and low velocity circumstellar matter generates photon emission that further affects the velocity distribution and the ionization and excitation of both the circumstellar matter and the SN ejecta. These interactions can produce a rich array of effects on the optical spectra. During the photospheric phase narrow emission, absorption, and P Cygni lines formed in low velocity circumstellar matter may be superimposed on the SN spectrum [8,9,112,116]. The SN resonance scattering features may be "muted" by the external illumination of the SN line forming region [14]. In extreme cases the circumstellar matter may be optically thick in the continuum so that the spectrum consists only of circumstellar features, perhaps including broad wings produced by multiple scattering off circumstellar electrons [21]. During the nebular phase CSI can power boxy emission from high velocity SN matter [42] and at very late times, even decades, CSI can allow the detection of SNe that would otherwise be unobservably faint [35].

Because the simple $r = vt$ velocity law does not apply to circumstellar matter, and blending of circumstellar lines generally is not as severe as it is for SN lines (and spherical symmetry often is not an adequate approximation for circumstellar matter), few calculations of synthetic spectra for CSI have been carried out so far. Line profiles for various velocity and density distributions have been calculated [40,23] and some `PHOENIX` calculations for a constant velocity circumstellar shell have been carried out [70]. Most of the analysis of optical CSI features has involved extracting information on velocities directly from individual line profiles, and on physical conditions and abundances from emission line fluxes [17,23,32,88].

2.4 Asymmetry and Polarization Spectra

It has been the heuristic and hopeful assumption that SNe are essentially spherically symmetric. But from SN polarimetry, especially spectropolarimetry, it is

now clear that all types of SNe other than SNe Ia usually do exhibit some kind of significant asymmetry (e.g, [61,78,130,132]).

The polarization of SN flux in most cases arises from their atmospheres where continuous opacity is dominated by electron scattering in the optical and near infrared. Electron scattering is polarizing with polarization (for incident unpolarized radiation) varying from 100 % for 90° scattering to 0 % for forward and backward scattering according to the Rayleigh phase matrix [16]. The polarization position angle is perpendicular to the scattering plane defined by incident and scattered light. The emergent flux from a deep electron scattering atmosphere (either plane-parallel or geometrically extended) tends to exhibit a position angle aligned perpendicular to the normal to the surface and polarization increasing monotonically from 0 % at an emission angle of 0° (to the normal) to a maximum at an emission angle of 90°. For the plane-parallel case the maximum is only 11.7 % [16], but for a highly extended atmosphere it can approach 100 % [15] from the limb, if it can be resolved. SN atmospheres fall into the extended class, and so beams from their limb should be highly polarized though mostly not at 100 %. Beams from the photodisk region (the projection of the photosphere on the sky) should be much less polarized. If SNe were spherically symmetric, the integrated flux (which is all that can be observed from extragalactic SNe) would have zero polarization since all polarization alignments would contribute equally and thus cancel producing zero net polarization. Because of cancellation, the predicted net continuum polarizations are low (a few percent: see below) even for quite strong asymmetries.

Line scattering is usually depolarizing [62]. The simplest line polarization profile is an inverted P Cygni profile that is common although not universal in the SN 1987A data [63] and is seen in some of the later spectropolarimetry [130]. In this profile a polarization maximum is associated with the P Cygni absorption feature of the flux spectrum and a polarization minimum is associated with the P Cygni flux emission feature. The inverted P Cygni profile has a natural explanation. The polarized flux at any wavelength tends to come from 90° electron scattering. At the flux absorption, unpolarized flux directly from the photosphere is scattered out of the line of sight by a line: thus, the electron polarized flux is less diluted and a polarization maximum arises. At the flux emission, the line scatters into the line of sight extra unpolarized flux diluting the polarization due to the electron scattered flux. Almost any shape asymmetry should tend to give the inverted polarization P Cygni profile. Thus, the inverted P Cygni profile is somewhat limited as a direct analysis tool for asymmetry.

Although one must be cautious in generalizing because of the paucity and inhomogeneity of published data, it seems that most core-collapse SNe that have been observed well enough to detect polarization of order a few tenths of percent (of order 40 to date) have shown at least that much continuum polarization. Some of this can be interstellar polarization (ISP) due to intervening dust, but intrinsic polarization seems to be present in many cases. The intrinsic polarization reveals itself through time dependence and, in spectropolarimetry, by line polarization features or by deviation from the ISP wavelength dependence [114].

Unfortunately, correcting for parent–galaxy ISP can only be done from an analysis of the SN data itself because there is no other bright nearby point source. Even the Galactic ISP correction may often have to be determined using the SN data since ISP can vary rapidly with position and depth and there may be no suitable Galactic star near the angular position of the SN. Techniques for correcting for ISP have been developed [61,63,77].

Fig. 2 shows a sample of spectropolarimetry from a range of SN types overlapping the corresponding relative flux spectra. The polarization has been corrected for ISP, but in most cases only with the intention of highlighting the line polarization features: the overall polarization level is not trustworthy. Some of the line polarization features are consistent with the inverted P Cygni profile. However, line polarization features are badly distorted by ISP, and thus reliable ISP corrections are needed to determine the true line polarization profiles as well as the true continuum polarization.

For core-collapse SNe the intrinsic continuum polarization varies from probably $\sim 0.0\,\%$ up to perhaps $\sim 4\,\%$ [74,130]: a representative value would be $1\,\%$. There may be a class of core-collapse SNe (those with massive hydrogen envelopes) that have nearly zero polarization at early times [74], and so are highly spherical. Apparent trends are that polarization increases with decreasing envelope mass (i.e., SNe II-P least polarized, SNe Ic most), and that polarization increases with time until the electron optical depth becomes small [63,76,130]. The position angle of polarization tends to be nearly constant in time and wavelength [63,76,130], which is naturally accounted for by axisymmetry in the ejecta.

For SNe Ia most observations (of order 15 to date) have only been able to place an upper limit of about $0.3\,\%$ continuum polarization (not distinguishing intrinsic from ISP in most cases) [132]. One normal event, SN 1996X, has a marginal detection of intrinsic polarization of $\sim 0.3\,\%$ [129]. Spectropolarimetry of SN 1997dt also may show the signatures of intrinsic polarization (Fig. 2). So far it seems that normal SNe Ia are not very polarized and are quite spherically symmetric: this is consistent with the observational homogeneity that makes them such useful tools for cosmology. On the other hand, the subluminous SN 1991bg-like event SN 1999by had intrinsic continuum polarization reaching up to perhaps $0.8\,\%$ [61]. Based on a sample of one, subluminous SNe Ia may be significantly asymmetric.

Various models of asymmetry have been presented to interpret the polarization data. The conventional model is axisymmetric ellipsoidal asymmetry, either prolate or oblate [56,62,97,115]. Even when viewed equator-on, considerable ellipsoidal asymmetry is required to account for SN-like continuum polarization. For example, Monte Carlo calculations suggest that iso-density contour axis ratios of order 1.2:1 and 2.5:1 are needed for polarizations of $1\,\%$ and $3\,\%$, respectively [58,130]. Late-time imaging of SN 1987A shows asymmetries suggesting axis ratios of 2:1 [57,131]. Thus large organized asymmetries something like the ellipsoidal models may account for most SN polarization. Other suggested models of polarizing large–scale asymmetry are asymmetric clumpy ionization [18], or scattering of SN light off a nearby dust cloud [128] or off bipolar jets [65].

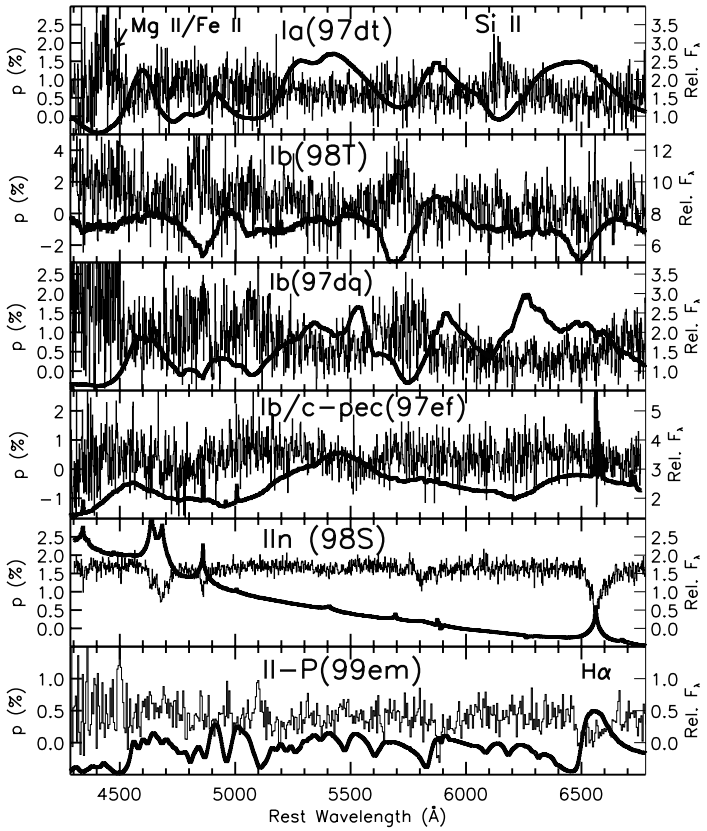

Fig. 2. Spectropolarimetry (*thin lines*) of various SN types, with the corresponding flux spectra (*thick lines*), all obtained within two months of explosion. Figure courtesy of D.C. Leonard

Spectropolarimetry plays an extremely important role in polarimetric observations for two reasons: (1) it is very useful for establishing intrinsic polarization and correcting for ISP, and (2) it is probably vital for understanding the SN asymmetry. Currently the most advanced synthetic polarization spectrum analyses are done with a 3-dimensional (3D) NLTE code that uses Monte Carlo radiative transfer in the outer region where emergent polarization is formed [57,61]. The NLTE component of these calculations is necessarily more limited than in 1D calculations since 3D radiative transfer calculations are computationally very demanding. The ellipsoidal asymmetry used in the calculations of [61] is parameterized and then fitted to the flux and polarization observations. Explosion model asymmetries can also be used [57]. Because of the large parameter space to explore in investigating SN asymmetry, less elaborate codes than

that of [57] and [61] will also continue to be useful. Such codes will mostly rely on Monte Carlo radiative transfer because of its flexibility and robustness.

In addition to the shape asymmetries discussed above, the ejected matter also may be "clumped" (see Chap. 15). Both observation and theory indicate that macroscopic (not microscopic) mixing is ubiquitous in SNe. Clumping is difficult to detect via polarization (although see [18]), but it can affect both the photospheric [22,33,34] and nebular [10,24,35,79,88,96] flux spectra. A version of `SYNOW` for calculating flux spectra with clumps (`CLUMPYSYN`) has been developed for analysis of the photospheric phase [122].

Circumstellar matter may, and probably often does, have both global asymmetry and clumping [24,32,42,74].

3 SNe Ia

SNe Ia are thought to be thermonuclear disruptions of accreting or merging white dwarfs. They can be separated on the basis of their photospheric spectra into those that are normal and those that are peculiar. Normals such as the recently well observed SNe 1996X [111] and 1998bu [54,67] have P Cygni features due to Si II, Ca II, S II, O I, and Mg II around the time of maximum brightness, and develop strong Fe II features soon after maximum. Peculiar, weak SN 1991bg–like events such as SNe 1998de [103], 1997cn [125], and 1999by [44,61,127] have, in addition, conspicuous low excitation Ti II features. Peculiar powerful SN 1991T–like events such as SNe 1997br [80] and 2000cx [81] have conspicuous high excitation Fe III features at maximum and the usual SN Ia features develop later. Events such as SN 1999aa [82] appear to link the 1991T–like events to the normals [11]. Nebular spectra of SNe Ia are dominated by collisionally excited forbidden emission lines of [Fe III], [Fe II], and [Co III]. SN Ia ejecta basically consist of a core of iron peak isotopes (initially mostly ^{56}Ni) surrounded by a layer of intermediate–mass elements such as silicon, sulfur, and calcium. Inferring the composition of the outermost layers is difficult [39,49,92,95] because the lines are broad and line formation occurs in these layers for only a short time after explosion.

Current viable hydrodynamical models for SNe Ia include deflagrations and delayed detonations (see Chap. 12 by S.E. Woosley). The composition structure of the classic deflagration model W7 [104,121] can account reasonably well for most of the photospheric and nebular spectral features of normal SNe Ia (Figs. 3 and 4). On the other hand, near infrared spectra appear to contain valuable diagnostics of the composition structure [10,54,98] and may provide evidence in favor of delayed detonation models [133].

SNe Ia can be arranged in a spectroscopic sequence ranging from the powerful SN 1991T–like events through the normals to the weak SN 1991bg–like events. The sequence usually is based on the R(Si II) parameter [105] – the ratio of the depth of an absorption feature near 5800 Å to that of the deep Si II absorption feature near 6100 Å. The ratio increases with decreasing temperature owing to the increasing contribution of numerous weak Ti II lines to the 5800 Å absorption

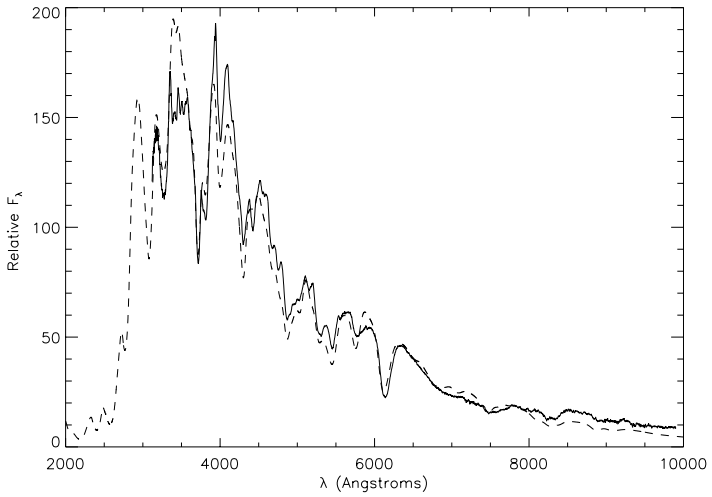

Fig. 3. The spectrum of the Type Ia SN 1994D three days before maximum brightness (*solid line*) and a `PHOENIX` synthetic spectrum for the deflagration model W7 17 days after explosion (*dashed line*) (From [72]).

[44] (Fig. 5). The velocity at the outer boundary of the iron peak core, as inferred from nebular spectra, also varies along the spectral sequence [90]. The principle physical variable along the sequence is thought to be the mass of ejected ^{56}Ni in a constant total ejected mass which is near the Chandrasekhar mass.

The lack of a clear correlation between R(Si II) and the blueshift of the 6100 Å feature shows that the diversity among SN Ia spectra actually is at least two dimensional [51]. Blueshift differences among events that have similar values of R(Si II) appear to be caused by differences in the amount of mass that is ejected at high velocity, $\sim 15,000-20,000\,\mathrm{km\,s^{-1}}$ [71] (Fig 6). One possibility is that the high velocity events are delayed detonations while the others are deflagrations.

The influence of metallicity on SN Ia spectra is of special interest in connection with the use of high redshift SNe Ia as distance indicators for cosmology. The main effects are in the ultraviolet but there also are some mild effects in the optical [59,73].

Deflagrations are expected to produce macroscopic mixing and clumping in the ejecta. The first application of the `CLUMPYSYN` code has shown that the uniformity of the observed depth of the 6100 Å Si II absorption in SNe Ia near maximum brightness provides limits on the sizes and numbers of clumps [122].

Although the polarization of most SNe Ia is low, the significant polarization of the SN 1991bg–like event SN 1999by (Fig. 7) raises the question of whether the production of weak SNe Ia may involve rapid white dwarf rotation or merging [61].

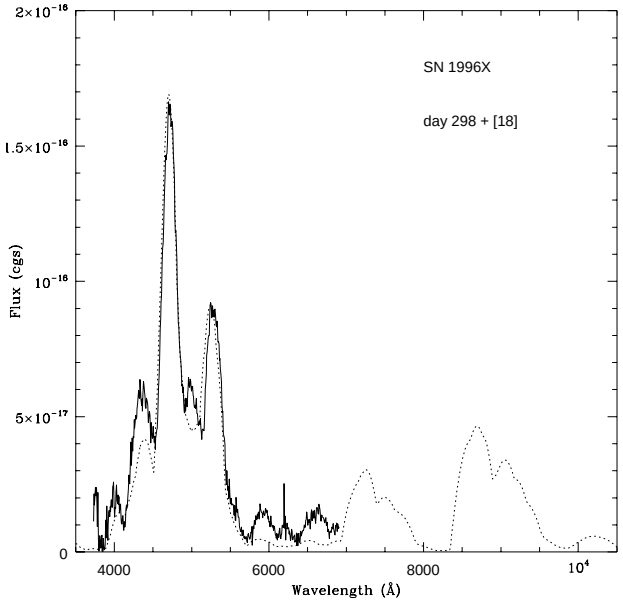

Fig. 4. The spectrum of the Type Ia SN 1996X 298 days after maximum brightness (*solid line*) is compared with a synthetic spectrum calculated with the `RL NEBULAR` code (*dotted line*) (From [111])

4 SNe Ib

SNe Ib are thought to result from core collapse in massive stars that have lost all or almost all of their hydrogen envelopes. The photospheric spectra contain the usual low excitation SN features such as Ca II and Fe II together with strong He I lines that are nonthermally excited by the decay products of ^{56}Ni and ^{56}Co [48,84,119]. Recent work on photospheric spectrum calculations includes a comparison of one NLTE synthetic spectrum of a hydrodynamic model with a spectrum of SN 1984L [135], a `SYNOW` study of line identifications in SN 1999dn [30], and a comparative `SYNOW` study of the spectra of a dozen SNe Ib [13].

`SYNOW` spectra can match the observed spectra rather well (Fig. 8). Consistent with the observational homogeneity of SNe Ib found by [89], the sample studied by [13] obeys a surprisingly tight relation between the velocity at the photosphere as inferred from Fe II lines and the time relative to maximum brightness. The masses and kinetic energies of the events in the sample appear to be similar, and not much room is left for any influence of departures from spherical symmetry on the velocity at the photosphere. After maximum brightness the He I lines usually are detached, but the minimum velocity of the ejected helium is at least as low as 7000 km s^{-1} (Fig. 9). The spectra of SNe 2000H, 1999di, and 1954A contain detached hydrogen absorption features forming at $\sim 12,000$ km s^{-1} (Fig. 9), and

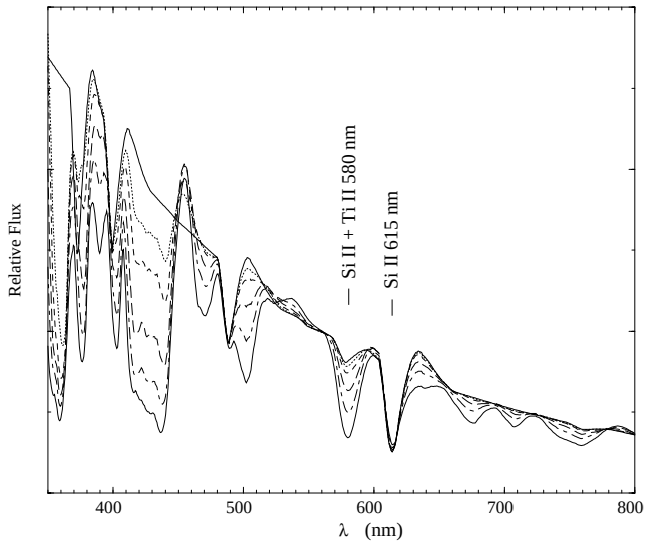

Fig. 5. `SYNOW` synthetic spectra with only Si II lines (*heavy line*) and also with Ti II lines of various strengths (*thin lines*). The 580 nm absorption is strongly affected by Ti II lines (From [44]).

hydrogen appears to be present in SNe Ib in general, although in most events it becomes too weak to identify soon after maximum brightness. The hydrogen line optical depths used to fit the spectra of SNe 2000H, 1999di, and 1954A are not high, so only a mild reduction would be required to make these events look like typical SNe Ib. Similarly, the He I line optical depths in typical SNe Ib are not very high, so a moderate reduction would make them look like SNe Ic.

The number of SNe Ib for which good spectral coverage is available is still small. More events need to be observed to explore the extent of the spectral homogeneity and to determine whether there is a continuum of hydrogen line strengths. Also needed are detailed NLTE calculations for hydrodynamical SN Ib models having radially stratified composition structures, to determine the hydrogen and helium masses and the distribution of the ^{56}Ni that excites the helium.

To our knowledge there have not been any synthetic spectrum calculations for the SN Ib nebular phase since 1989 [43]. Most of the recent effort has been devoted to inferring the composition from emission line profiles and fluxes [89].

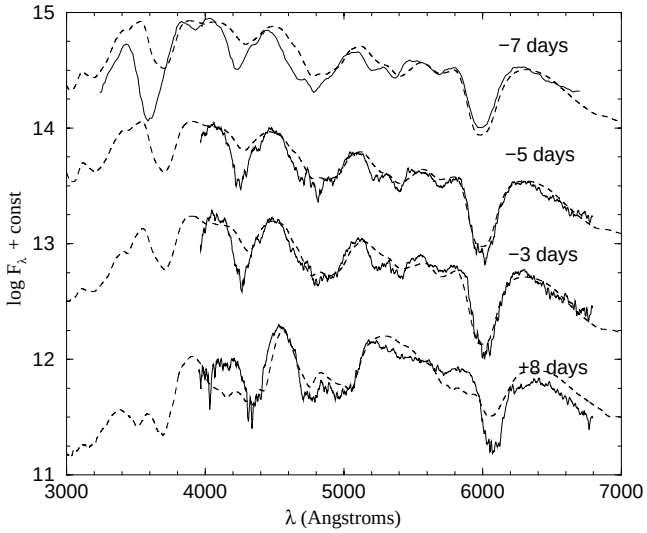

Fig. 6. `PHOENIX` synthetic spectra for the delayed detonation model CS15DD3 (*dashed lines*) and observed spectra of the high-velocity Type Ia SN 1984A (*solid lines*). (From [71])

The oxygen mass, evidence for hydrogen, and evidence for asymmetry from the nebular spectra of SN 1996N have been discussed by [117].

5 SNe Ic

SNe Ic are thought to result from core collapse in massive stars that either have lost their helium layer or fail to nonthermally excite their helium. If the helium layer is gone, the outer layers of the ejected matter are expected to be mainly carbon and oxygen. SNe Ic are spectroscopically more diverse than SNe Ib [28,89]. The photospheric spectra are dominated by the low excitation SN features that appear in SNe Ib. The spectra of the best studied ordinary Type Ic, SN 1994I, can be reasonably well matched by `SYNOW` spectra [100] (Fig. 10). Discrepancies between the SN 1994I spectra and `PHOENIX` spectra indicate that the appropriate hydrodynamical model for SN 1994I has not yet been found [5]. The important issue of whether helium is detectable in SN Ic spectra is not yet resolved, because an absorption near 10,000 Å that sometimes is attributed to He I λ10,830 could be produced by one of several other ions (see Fig. 10 and [5,100]), and identifications of very weak optical lines [26] are difficult to confirm [89].

The peculiar, hyperenergetic Type Ic SN 1998bw that was associated with a gamma ray burst is discussed in Chap. 25. SN 1997ef was a less extreme example of a hyperenergetic SN Ic. The spectra of these events, although difficult to interpret because of the severe Doppler broadening and blending, can be

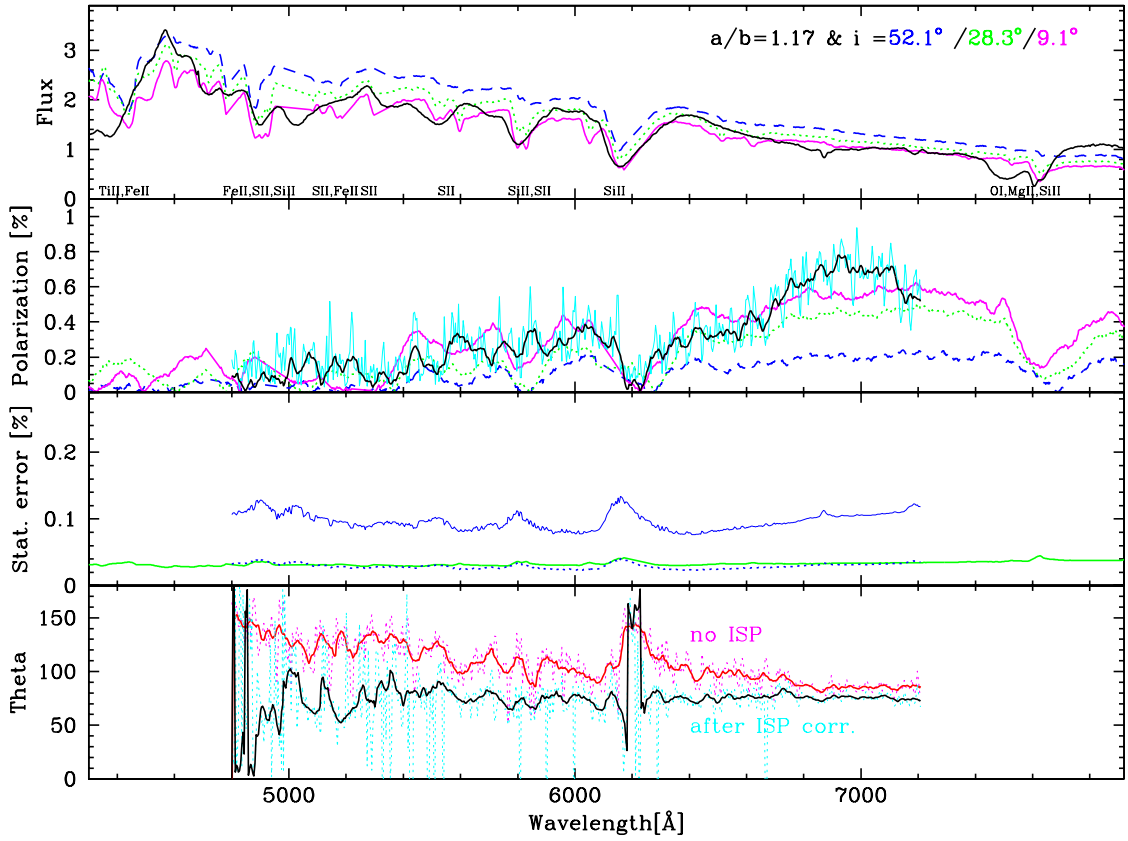

Fig. 7. Flux spectra (*top panel, black line*) and raw and smoothed polarization spectra (*second panel, light blue and black lines*) of the peculiar weak Type Ia SN 1999by near maximum brightness, are compared with synthetic spectra computed for an oblate ellipsoidal model with axis ratio 1.17 and three inclinations of the symmetry axis from the line of sight. (From [61], where further explanation of this figure can be found)

matched fairly well by the `SYNOW` [12] and `ML MONTE CARLO` codes [94] (Fig. 11), and the resulting spectroscopic estimates of the kinetic energy (in the spherical approximation) are far in excess of the canonical 10^{51} ergs [12,94,96,106]. Detailed NLTE synthetic spectrum calculations have not yet been carried out for the photospheric spectra of hyperenergetic SNe Ic, and the only recent synthetic spectrum calculations for nebular phase SNe Ic have been for SN 1998bw with the `RL NEBULAR` code [96] (see Chap. 25).

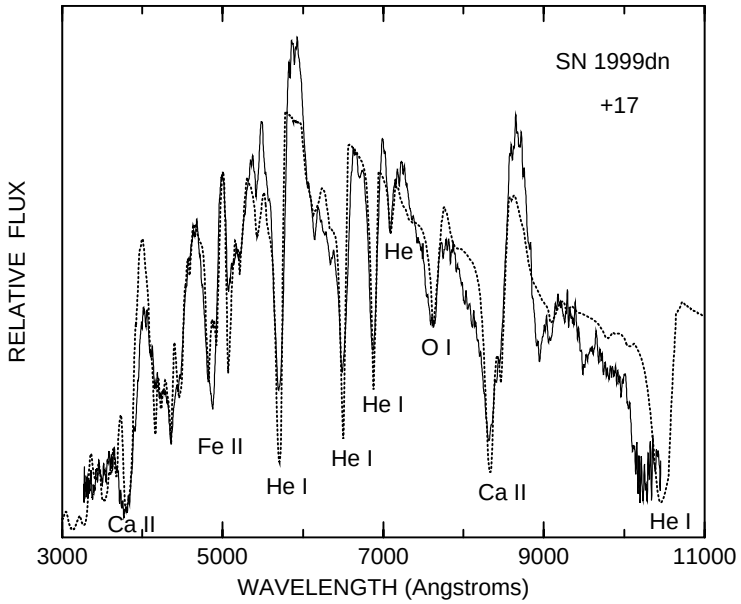

Fig. 8. The spectrum of the Type Ib SN 1999dn 17 days after maximum brightness (*solid line*) is compared with a `SYNOW` synthetic spectrum (*dotted line*) that has $v_{phot} =$ 6000 km s^{-1}. (From [13])

The Type Ic SN 1999as, one of the most luminous reliably measured SNe to date, contained highly blueshifted ($\sim 11,000$ km s^{-1}) but narrow (~ 2000 km s^{-1}) absorption features [52] that cannot be produced by spherically symmetric SN ejecta. Whether these unusual features are produced by an ejecta clump in front of the photosphere or by circumstellar matter accelerated by the SN is not yet clear.

Detailed NLTE calculations for hydrodynamical models of typical and hyperenergetic SNe Ic are needed, to constrain the helium mass and the ejected mass and kinetic energy.

6 SNe II

SNe II are the most spectroscopically diverse of the SN types, partly because the optical effects of CSI range from negligible in some events to dominant in others. In the absence of CSI and the presence of a substantial hydrogen envelope (SNe II-P and II-L) the spectrum evolves from an almost featureless continuum when the temperature is high to one that contains first hydrogen and helium lines and then also the usual low excitation lines as the temperature falls. The photospheric spectra of SN 1987A were, of course, extensively studied [31,55,66,113]. Recently it has been shown that the observed profile of the He I λ10830 line in SN 1987A is a sensitive probe of the degree of mixing of ^{56}Ni

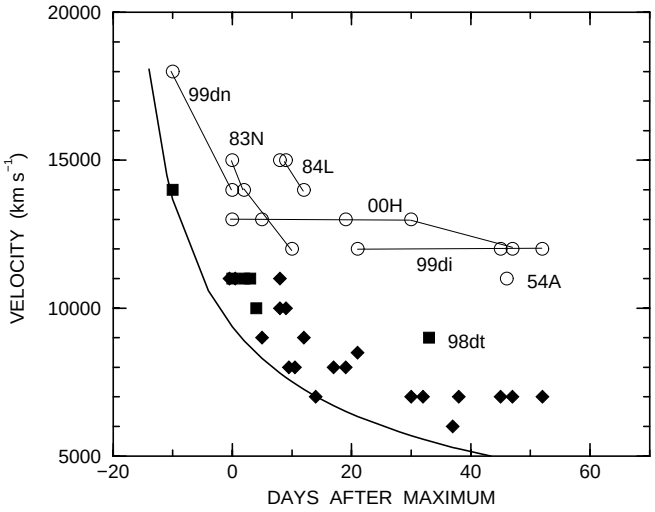

Fig. 9. For a sample of 12 SNe Ib, the minimum velocity of the He I lines (*filled squares* when undetached, *filled diamonds* when detached) and the minimum velocity of the hydrogen lines (*open circles*, always detached) are plotted against time after maximum brightness. The *heavy curve* is a power law fit to the velocity at the photosphere as determined by Fe II lines. (From [13])

out to relatively high velocities, $\sim$ 3000 km s^{-1} [33] (see also [34] for similar work on the Type II-P SN 1995V). `PHOENIX` calculations [102] show that the hydrogen lines of SN 1987A also are a sensitive probe of the nickel mixing and may require some ^{56}Ni as fast as 5000 km s^{-1}. As discussed in these three papers, quantitative conclusions are sensitive to the details of the macroscopic mixing of the hydrogen, helium, and nickel.

SN 1999em is a recent SN II-P that has been extremely well observed and that is not complicated by CSI or large departures from spherical symmetry [76]. HST ultraviolet spectra [4] of this event are discussed in Chap. 7. Two extensive independent sets of optical spectra and photometry have been used to apply the expanding photosphere method for determining the distance [47,75]. `SYNOW` and `PHOENIX` synthetic spectra have been compared to the photospheric spectra [4]. Complicated observed P Cygni profiles of hydrogen and He I lines are well reproduced by the `PHOENIX` calculations when the density gradient is sufficiently shallow (Fig. 12). The total extinction can be inferred by comparing the observed and synthetic spectra at early times when the temperature is high [4].

The unusually weak Type II-P SN 1997D has attracted considerable attention in connection with the possibility of black hole formation and fallback. The `ML MONTE CARLO` code has been used to fit the spectrum with an extremely low velocity at the photosphere of only 970 km s^{-1} [123]. It has been pointed out that because of the unusually low ionization, Rayleigh scattering may have significant

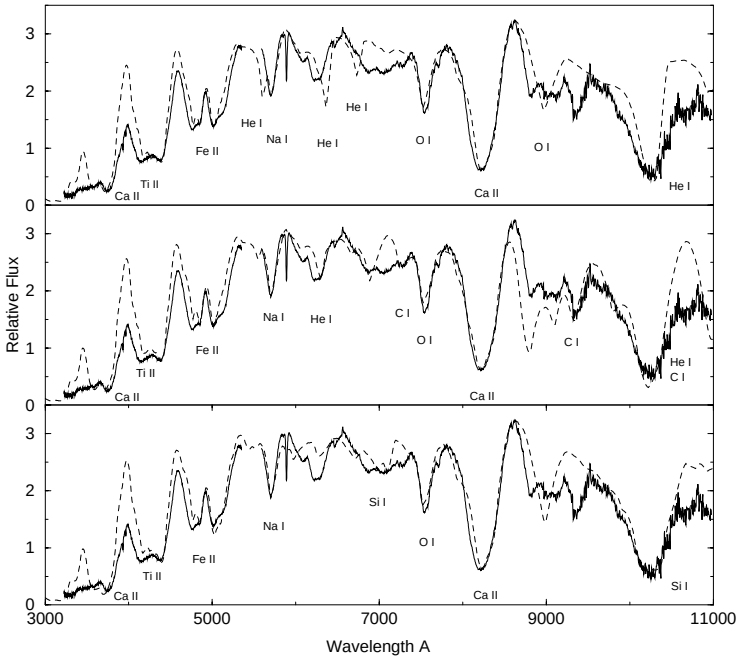

Fig. 10. The spectrum of the typical Type Ic SN 1994I 7 days after maximum brightness is compared with three `SYNOW` synthetic spectra that have $v_{phot} = 10,000$ km s^{-1}. To account for the observed infrared feature, the synthetic spectra include He I lines detached at 15,000 km s^{-1} (*top*); undetached C I lines and He I lines detached at 18,000 km s^{-1} (*middle*); and Si I lines detached at 14,000 km s^{-1} (*bottom*). (From [100])

effects on the photospheric spectrum [25]. The low expansion velocity offered a unique opportunity to identify lines in the nebular spectra [7]. Nebular synthetic spectra have been calculated [25] and it has been pointed out that the Sobolev approximation may break down in the early nebular phase because Hα damping wings can have significant effects [20].

SNe IIb contain conspicuous hydrogen lines at early times but not at late times, indicating that these events lost nearly all of their hydrogen before exploding. In the well studied SN 1993J, He I lines became conspicuous after maximum brightness, as the hydrogen lines faded. The photospheric and nebular spectra were modeled in detail ([2,58,60,126] and references therein). More recent work on SN 1993J has concentrated on inferring properties of the clumps and the nature of the CSI directly from line profiles and fluxes [88]. A `SYNOW` line-identification study of extensive observations of the Type IIb SN 1996cb [108] has been carried out [29].

SNe IIn have narrow lines that form in low velocity circumstellar matter. Optical and infrared spectra of SN 1998S have been intensively studied [1,32,70,77,23]. HST ultraviolet spectra [70] are discussed in Chap. 7. `PHOENIX` synthetic spectra calculated for a simple model of the circumstellar shell accounted reasonably

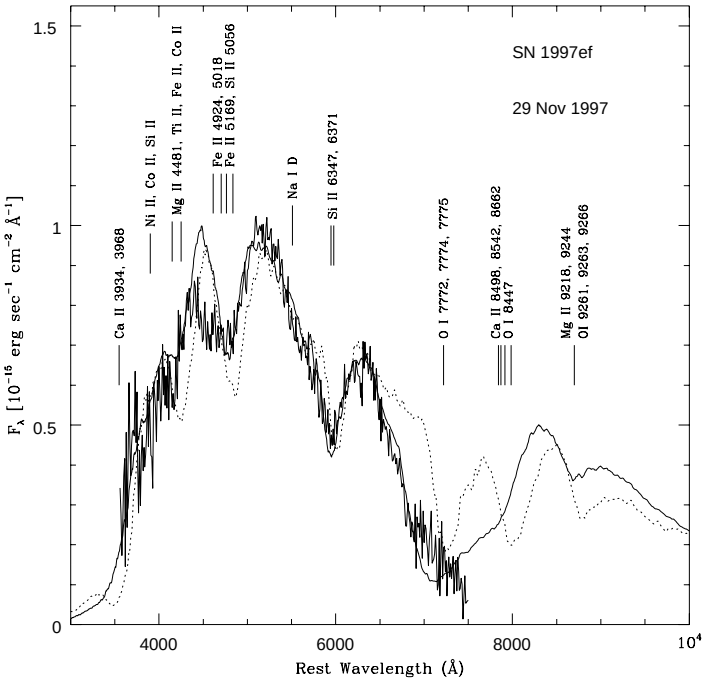

Fig. 11. The spectrum of the hyperenergetic Type Ic SN 1997ef about 11 days before maximum brightness(*thick line*) is compared with two synthetic spectra calculated with the `ML MONTE CARLO` code. The *thin solid line* and the *dotted line* are for models having kinetic energies of 8×10^{51} and 1.75×10^{52} erg, respectively. (From [94])

well for the early circumstellar-dominated spectra (Fig. 13). The inferences from spectroscopy are that the progenitor of SN 1998S underwent several distinct mass loss episodes during the decades and centuries before explosion, and that the SN ejecta or the circumstellar matter (or both) were significantly asymmetric. A detailed study of the nebular spectra of the Type IIn SN 1995N has revealed the existence of three distinct kinematic components (Fig. 14 shows nebular phase synthetic spectra calculated for the ~ 5000 km s^{-1} intermediate–velocity component that corresponds to unshocked SN ejecta) and produced the suggestion that SNe IIn are produced by red supergiants that collapse during their superwind phases [42] (see also [19]).

Synthetic spectra have not yet been compared to spectra of hyperenergetic SNe IIn such as SNe 1997cy [46,124] and SN 1999E [37], both of which may have been associated with gamma ray bursts. These events may prove to be related to SN 1988Z, which has been modeled in terms of CSI involving either dense clumps or a dense equatorial wind [24].

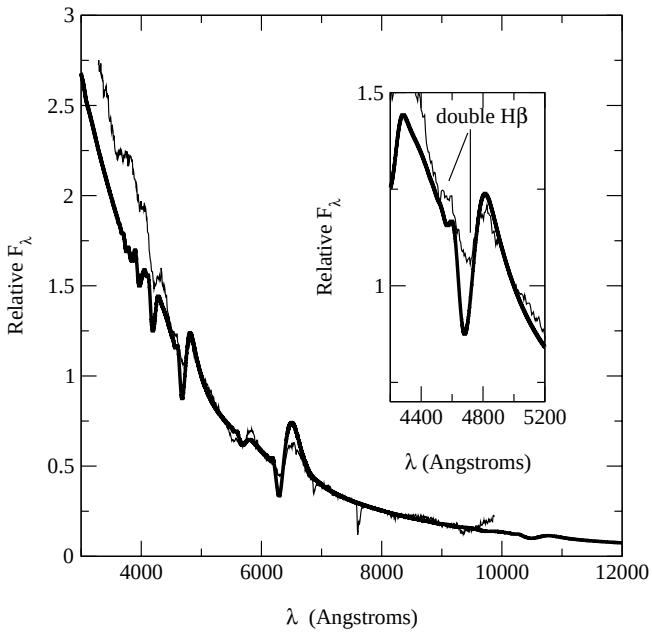

Fig. 12. The spectrum of the Type II SN 1999em four days before maximum brightness (*thin line*) is compared to a `PHOENIX` synthetic spectrum (*thick line*) with $Z = Z_\odot/100$. All lines in the synthetic spectrum are produced by hydrogen and helium. The inset shows a shoulder in both the observed and calculated Hβ profiles. (From [4])

7 Prospects

Observationally, in addition to a large increase in the sheer number of optical spectra, we can look forward to more and better infrared and nebular spectra, spectra obtained shortly after explosion, and spectropolarimetry.

Fast spherically symmetric (1D) photospheric–phase codes such as `SYNOW` and `ML MONTE CARLO` will continue to be valuable for making rapid interpretations of new flux spectra and for certain comparative studies. Monte Carlo 1D NLTE codes may be constructed [86]. As computational resources permit, detailed 1D codes such as `PHOENIX` will be used to generate large grids of models and spectra to expedite the comparison with observed spectra. `PHOENIX` will be modified to take into account the radiative coupling between circumstellar matter and SN ejecta, and as forbidden lines are added to the line list `PHOENIX` also will become a powerful 1D nebular–phase code.

The major challenge for the future is to develop codes for calculating spectra for arbitrary geometries (3D) of both the SN ejecta and the circumstellar matter (and learning how to use such codes effectively). For flux spectra, the already existing `CLUMPYSYN` code will be followed in the near future by 3D Monte Carlo codes and, eventually, by 3D `PHOENIX`–level codes. Spectropolarization calculations for 3D configurations are certain to emerge as a major focus of SN

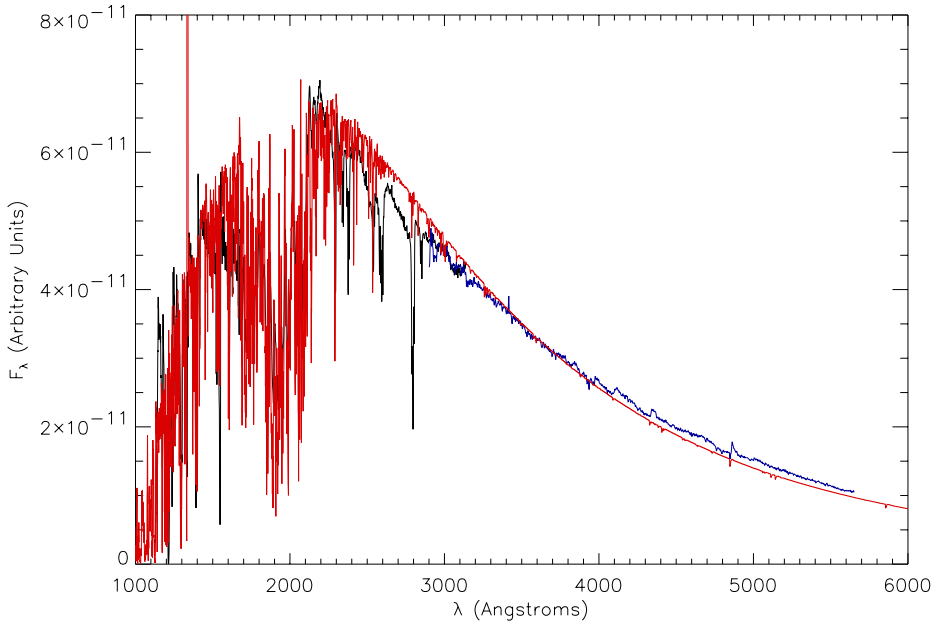

Fig. 13. The UV (*black line*) and optical (*blue line*) spectra of the Type IIn SN 1998S about four days before maximum brightness are compared with a `PHOENIX` synthetic spectrum (*red line*) calculated for a circumstellar shell having an r^{-2} density distribution and a constant expansion velocity of 1000 km s^{-1}. (From Len01a)

spectroscopy; Monte Carlo codes for calculating 3D polarization spectra also will become available in the near future.

We are grateful to Doug Leonard for providing an unpublished figure, and to him and Lifan Wang for helpful comments. This work was supported by NASA, NSF, and the Physics Department of New Mexico Tech.

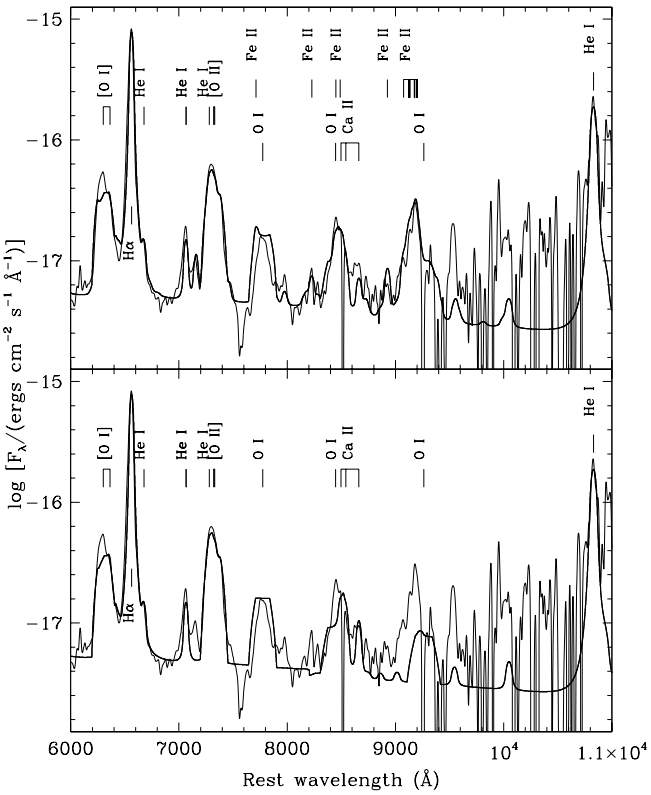

Fig. 14. The spectrum of the Type IIn SN 1995N nearly five years after maximum brightness is compared to synthetic spectra calculated with (*upper*) and without (*lower*) the influence of Lyα fluorescence on the Fe II lines taken into account. (From [42])

References

1. G.C. Anupama, T. Sivarani, G. Pandey: A&A **367**, 506 (2001)
2. E. Baron et al.: ApJ **441**, 170 (1995)
3. E. Baron, P.H. Hauschildt, A. Mezzacappa: MN **278**, 763 (1996)
4. E. Baron et al.: ApJ **545**, 444 (2000)
5. E. Baron, D. Branch, P.H. Hauschildt, A.V. Filippenko, R.P. Kirshner: ApJ **527**, 739 (1999)
6. E. Baron, P.H. Hauschildt, P. Nugent, D. Branch: MN **283**, 297 (1996)
7. S. Benetti et al.: MN **322**, 361 (2001)
8. S. Benetti, E. Cappellaro, I.J. Danziger, M. Turatto, F. Patat, M. Della Valle: MN **294**, 448 (1998)
9. S. Benetti, M. Turatto, E. Cappellaro, I.J. Danziger, P.A. Mazzali: MN **305**, 811 (1999)
10. E.J.C. Bowers et al.: MN **290**, 663 (1997)
11. D. Branch: PASP **113**, 169 (2001)
12. D. Branch: 'Direct Analysis of Spectra of Type Ic Supernovae'. In: *Supernovae and Gamma Ray Bursts, Space Telescope Science Institute Symposium on Supernovae and Gamma Ray Bursts, at Baltimore, MD, USA, May 3–6, 1999*, ed. by M. Livio, N. Panagia, K. Sahu (Cambridge University, Cambridge 2001) p. 96
13. D. Branch et al.: ApJ **566**, in press (2002)
14. D. Branch, D.J. Jeffery, M. Blaylock, K. Hatano: PASP **112**, 217 (2000)
15. J.P. Cassinelli, D.A. Hummer: MN **154**, 9 (1971)
16. S. Chandrasekhar: *R*adiative Transfer (Dover Publications, New York 1960)
17. R.A. Chevalier, C. Fransson: ApJ **420**, 268 (1994)
18. N.N. Chugai: 1992, Sov. Astron. Lett. **18(3)**, 168 (1992)
19. N.N. Chugai: Astr. Rep. **41**, 672 (1997)
20. N.N. Chugai: ApJ **531**, 411 (2000)
21. N.N. Chugai: ApJ **326**, 1448 (2001)
22. N.N. Chugai, A.A. Andronova, V.P. Utrobin: Astr. Lett. **22**, 672 (1996)
23. N.N. Chugai, S.I. Blinnikov, A. Fassia, P. Lundqvist, W.P.S. Meikle, E.I. Sorokina: MNRAS, in press (2002)
24. N.N. Chugai, I.J. Danziger: MN **268**, 173 (1994)
25. N.N. Chugai, V.P. Utrobin: A&A **354**, 557 (2000b)
26. A. Clocchiatti et al: ApJ **483**, 675 (1997)
27. A. Clocchiatti et al: ApJ **529**, 661 (2000)
28. A. Clocchiatti et al: ApJ **553**, 886 (2001)
29. J.S. Deng, Y.L. Qiu, J.Y. Hu: ApJ, submitted (2001)
30. J.S. Deng, Y.L. Qiu, J.Y. Hu, K. Hatano, D. Branch: ApJ **540**, 452 (2000)
31. R. Eastman, R.P. Kirshner: ApJ **347**, 771 (1989)
32. A. Fassia et al.: MN **325**, 907 (2001)
33. A. Fassia, W.P.S. Meikle: MN **302**, 314 (1999)
34. A. Fassia, W.P.S. Meikle, T.R. Geballe, N.A. Walton, D.L. Pollacco, R.G.M. Rutten, C. Tinney: MN **299**, 150 (1998)
35. R. Fesen et al.: AJ **117**, 725 (1999)
36. A.V. Filippenko: ARAA **35**, 309 (1997)
37. A.V. Filippenko: 'Optical Observations of Type II Supernovae'. In: *Cosmic Explosions, 10th Annual October Astrophysics Conference, at College Park, MD, October 11-13, 1999*, ed. by S. Holt, W.W. Zhang (AIP, New York 2000)

38. A.K. Fisher: Direct Analysis of Type Ia Supernova Spectra. PhD Thesis, University of Oklahoma, Norman (2000)
39. A.K. Fisher, D. Branch, K. Hatano, E. Baron: MN **304**, 67 (1999)
40. C. Fransson: A&A **132**, 115 (1984)
41. C. Fransson: 'The Late Emission from Supernovae'. In: *Supernovae, NATO Advanced Study Institute on Supernovae, at Les Houches, France, July 31–September 1, 1990*, ed. by S.A. Bludman, R. Mochkovitch, J. Zinn-Justin (Elsevier, Amsterdam 1994) p. 677
42. C. Fransson et al.: ApJ, in press (2001)
43. C. Fransson, R.A. Chevalier: ApJ **343**, 323 (1989)
44. P.M. Garnavich et al.: ApJ, in press (2001)
45. C.L. Gerardy, R.A. Fesen, P. Höflich, J.C. Wheeler: AJ **119**, 2968, (2000)
46. L.M. Germany, D.J. Riess, E.M. Sadler, B.P. Schmidt, C.W. Stubbs: ApJ **533**, 320, (2000)
47. M. Hamuy et al.: ApJ **558**, 615 (2001)
48. R.P. Harkness et al.: ApJ **317**, 355 (1987)
49. K. Hatano, D. Branch, A. Fisher, E. Baron, A. V. Filippenko: ApJ **525**, 881 (1999)
50. K. Hatano, D. Branch, A. Fisher, J. Millard, E. Baron: ApJ Suppl. **121**, 233 (1999)
51. K. Hatano, D. Branch, E.J. Lentz, E. Baron, A.V. Filippenko, P.M. Garnavich: ApJ **543**, L49 (2000)
52. K. Hatano, D. Branch, K. Nomoto, J.S. Deng, K. Maeda, P. Nugent, G. Aldering: BAAS **198**, 3902 (2001)
53. P.H. Hauschildt, E. Baron: J. Comp. Appl. Math. **109**, 41 (1999)
54. M. Hernandez et al.: MN **319**, 223 (2000)
55. P. Höflich : Proc. Astron. Soc. Aust. **7**, 434 (1988)
56. P. Höflich: A&A **246**, 481 (1991)
57. P. Höflich, A. Khokhlov, L. Wang: 'Aspherical Supernova Explosions: Hydrodynamics, Radiation Transport, & Observational Consequences'. In: *Relativistic Astrophysics, 20th Texas Symposium on Relativistic Astrophysics, at Austin, TX, December 10-15, 2000*, ed. by J.C. Wheeler, H. Martel (New York, AIP, 2001) p. 459
58. P. Höflich, J.C. Wheeler, D.C. Hines, S.R. Tramell: ApJ **459**, 307 (1996)
59. P. Höflich, J.C. Wheeler, F.K. Thielemann: ApJ **495**, 617 (1998)
60. J.C. Houck, C. Fransson: ApJ **456**, 811 (1996)
61. D.A. Howell, P. Höflich, L. Wang, J.C. Wheeler: ApJ **556**, 302 (2001)
62. D.J. Jeffery: ApJS **71**, 951 (1989)
63. D.J. Jeffery: ApJS **77**, 405 (1991)
64. D.J. Jeffery: ApJ **415**, 734 (1993)
65. D.J. Jeffery: ApJ, submitted (2001)
66. D.J. Jeffery, D. Branch: 'Analysis of Supernova Spectra'. In: *Supernovae, 6th Jerusalem Winter School for Theoretical Physics, at Jerusalem, Israel, December 28, 1988–January 5, 1989*, ed. by J.C. Wheeler, T. Piran, S. Weinberg (World Scientific, Singapore 1990) p. 149
67. S. Jha et al.: ApJ Suppl. **125**, 73 (1999)
68. A.H. Karp, G. Lasher, K.L. Chan, E.E. Salpeter: ApJ **214**, 161 (1977)
69. D. Kasen, D. Branch, E. Baron, D.J. Jeffery: ApJ, in press (2001)
70. E.J. Lentz et al.: ApJ **547**, 406 (2001)
71. E.J. Lentz, E. Baron, D. Branch, P. Hauschildt: ApJ **547**, 402 (2001)
72. E.J. Lentz, E. Baron, D. Branch, P. Hauschildt: ApJ **557**, 266 (2001)
73. E.J. Lentz, E. Baron, D. Branch, P. Hauschildt, P.E. Nugent: ApJ **530**, 966 (2000)
74. D.C. Leonard et al.: PASP, in press (2001)

75. D.C. Leonard, A.V. Filippenko: PASP **113**, 920 (2001)
76. D.C. Leonard, A.V. Filippenko, D.R. Ardila, M.S. Brotherton: ApJ **553**, 861 (2001)
77. D.C. Leonard, A.V. Filippenko, A.J. Barth, T. Matheson: ApJ **536**, 239 (2000)
78. D.C. Leonard, A.V. Filippenko, T. Matheson: 'Probing the Geometry of Supernovae with Spectropolarimetry'. In: *Cosmic Explosions, 10th Annual October Astrophysics Conference at College Park, MD, October 11-13, 1999*, ed. by S. Holt, W. W. Zhang (AIP, New York 2000), p. 165
79. H. Li, R. McCray, R.A. Sunyaev: ApJ **419**, 824 (1993)
80. W.D. Li et al.: ApJ **117**, 2709 (1999)
81. W.D. Li et al.: PASP **113**, 1178 (2001)
82. W.D. Li, A.V. Filippenko, R.R. Treffers, A.G. Riess, J. Hu, Y. Qiu: ApJ **546**, 734 (2000)
83. W. Liu, D.J. Jeffery, D.R.Schultz: ApJ **494**, 812 (1998)
84. L.B. Lucy: ApJ **383**, 308 (1991)
85. L.B. Lucy: A&A **345**, 211 (1999)
86. L.B. Lucy: MN **326**, 95 (2001)
87. T. Matheson, A.V. Filippenko, R. Chornock, D.C. Leonard, W. Li: AJ **119**, 2303 (2000)
88. T. Matheson, A.V. Filippenko, Ho, L.C., Barth, A.J., D.C. Leonard: AJ **120**, 1499 (2000)
89. T. Matheson, A.V. Filippenko, W. Li, D.C. Leonard, J.C. Shields: AJ **121**, 1648 (2001)
90. P.A. Mazzali: ApJ **499**, L49 (1998)
91. P.A. Mazzali: A&A **363**, 705 (2000)
92. P.A. Mazzali: MN **321**, 341 (2001)
93. P.A. Mazzali, N. Chugai, M. Turatto, L.B. Lucy, I.J. Danziger, E. Cappellaro, M. Della Valle, S. Benetti: MN **284**, 151 (1997)
94. P.A. Mazzali, K. Iwamoto, K. Nomoto: ApJ **545**, 407 (2000)
95. P.A. Mazzali, L.B. Lucy: MN **295**, 428 (1998)
96. P.A. Mazzali, K. Nomoto, F. Patat, K. Maeda: ApJ 559, 1047 (2001)
97. M.L. McCall: MN **210**, 829 (1984)
98. W.P.S. Meikle et al.: MN **281**, 263 (1996))
99. D. Mihalas: *S*tellar Atmospheres, (W. H. Freeman, San Francisco 1978)
100. J. Millard et al.: ApJ **527**, 746 (1999)
101. P.A. Milne, L.-S. The, M.D. Leising: ApJ **559**, 1019 (2001)
102. R. Mitchell, E. Baron, D. Branch, P. Lundqvist, S. Blinnikov, P.H. Hauschildt, C.S.J. Pun: ApJ **556**, 979 (2001)
103. M. Modjaz, W. Li, A.V. Filippenko, J.Y. King, D.C. Leonard, T. Matheson, R.R. Treffers: PASP **113**, 308 (2001)
104. K. Nomoto, F.-K. Thielemann, Y. Yokoi: ApJ **286**, 644 (1984)
105. P. Nugent, M.M. Phillips, E. Baron, D. Branch, P. Hauschildt: ApJ **455**, L147 (1995)
106. F. Patat et al.: ApJ **555**, 900 (2001)
107. P. Pinto, R.G. Eastman:: ApJ **530**, 757 (2000)
108. Y. Qiu, W. Li, Q. Qiao, J. Hu: AJ **117**, 736 (1999)
109. P. Ruiz-Lapuente: ApJ **439**, 60 (1995)
110. P. Ruiz-Lapuente, L.B. Lucy: ApJ **400**, 127 (1992)
111. M.E. Salvo, E. Cappellaro, P.A. Mazzali, S. Benetti, I. J. Danziger, M. Turatto: MN **321**, 254 (2001)
112. I. Salamanca, R. Cid-Fernandes, G. Tenorio-Tagle, E. Telles, R.J. Terlevich, C. Munoz-Tunon: MN **300**, 17 (1998)

113. W. Schmutz, D.C. Abbott, R.S. Russell, W.-R. Hamann, U. Wessolowski: ApJ **355**, 255 (1990)
114. K. Serkowski: In *Interstellar Dust and Related Topics, IAU Symposium 52, at Albany, NY, May 29 – June 2, 1972* ed. by J. M. Greenberg, H. C. van de Hulst (Reidel, Dordrecht 1973), p. 145
115. P.R. Shapiro, P.G. Sutherland: ApJ **263**, 902 (1982)
116. J. Sollerman, R.J. Cumming, P. Lundqvist: A&A **493**, 933 (1998)
117. J. Sollerman, B. Leibundgut, J. Spyromilio: A&A **337**, 207 (1998)
118. J. Spyromilio, B. Leibundgut, R. Gilmozzi: A&A **376**, 188 (2001)
119. D.A. Swartz, A.V. Filippenko, K. Nomoto, J.C. Wheeler: ApJ **411**, 313 (1993)
120. D.A. Swartz, P.G. Sutherland, R.P. Harkness J.C. Wheeler: ApJ **446**, 766 (1995)
121. F.-K. Thielemann, K. Nomoto, K. Yokoi: A&A, **158**, 17 (1986)
122. R.C. Thomas, D. Kasen, D. Branch, E. Baron: ApJ **567**, in press (2002)
123. M. Turatto et al.: ApJ **498**, L129 (1998)
124. M. Turatto et al.: ApJ **534**, L57 (2000)
125. M. Turatto, A. Piemonta, S. Benetti, E. Cappellaro, P.A. Mazzali, I.J. Danziger, F. Patat: AJ **116**, 2431 (1998)
126. V.P. Utrobin: A&A **306**, 231 (1996)
127. J. Vinkó, L.L. Kiss, B. Csák, G. Fürész, R. Sxabó, J.R. Thomson, S.W. Mochnacki: **121**, 3127 (2001)
128. L. Wang, J.C. Wheeler: ApJ **462**, L27 (1996)
129. L. Wang, J.C. Wheeler, P. Höflich: ApJ **476**, L27 (1997)
130. L. Wang, D.A. Howell, P. Höflich, J.C. Wheeler: ApJ **550**, 1030 (2001)
131. L. Wang et al.: Nature, submitted (2001)
132. J.C. Wheeler, S. Benetti: 'Supernovae'. In: *A*llen's Astrophysical Quantities, 4th Edition, ed. by A. N. Cox (Springer, New York 2000), p. 451
133. J.C. Wheeler, P. Höflich, R.P. Harkness, J. Spyromilio: ApJ **496**, 908 (1998)
134. J.C. Wheeler, D.A. Swartz, R.P. Harkness: Phys. Rep. **227**, 113 (1993)
135. S.E. Woosley, R.G Eastman: 'Type Ib and Ic Supernovae: Models and Spectra'. In: *Thermonuclear Supernovae, NATO Advanced Study Institute on Thermonuclear Supernovae, at Aiguablava, Spain, June 20–30, 1995*, ed. by P. Ruiz-Lapuente, R. Canal, J. Isern (Kluwer, Dordrecht 1997) p. 821

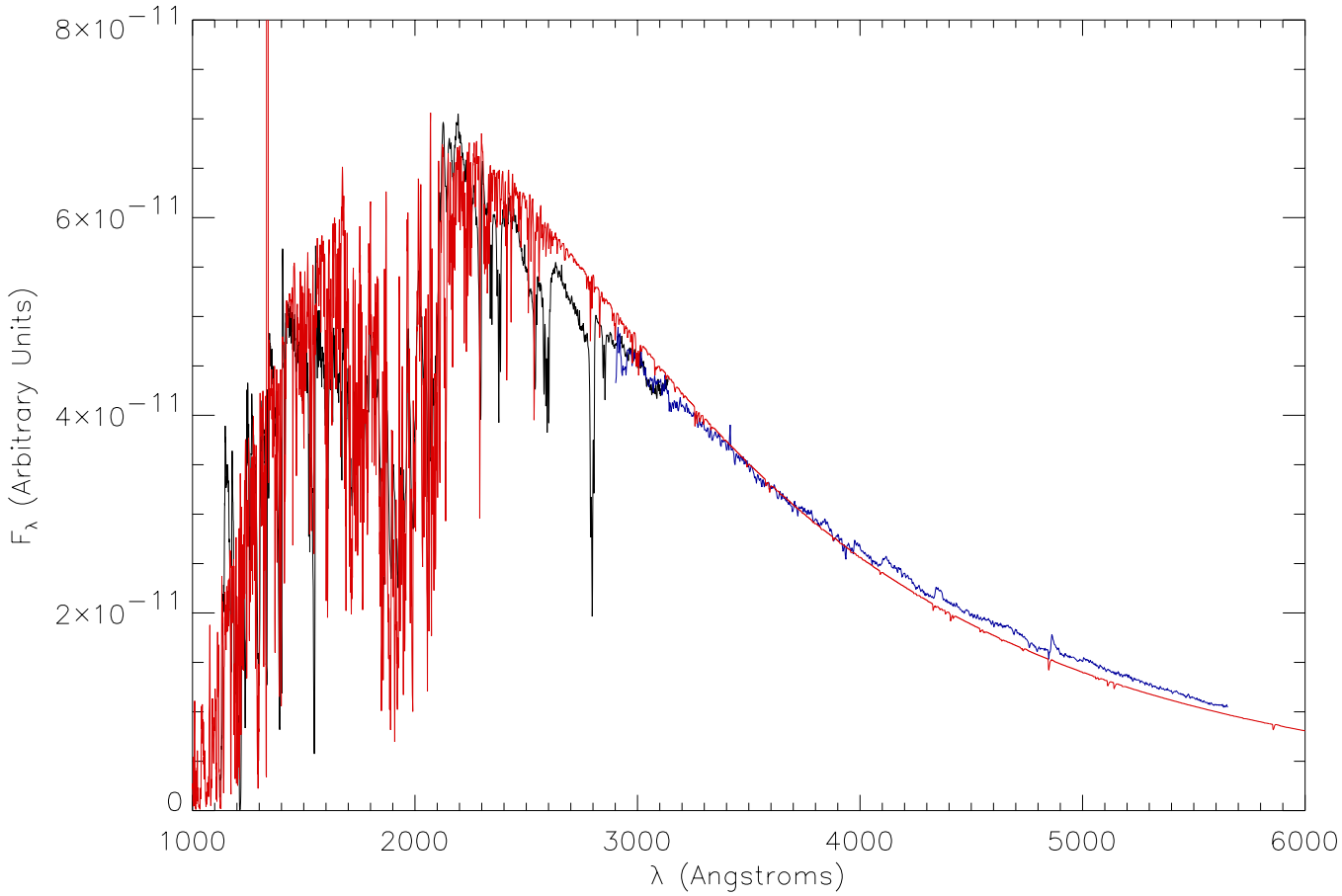
8×10⁻¹¹
6×10⁻¹¹
4×10⁻¹¹
2×10⁻¹¹
0
Fλ (Arbitrary Units)
1000
2000
3000
4000
5000
6000
λ (Angstroms)

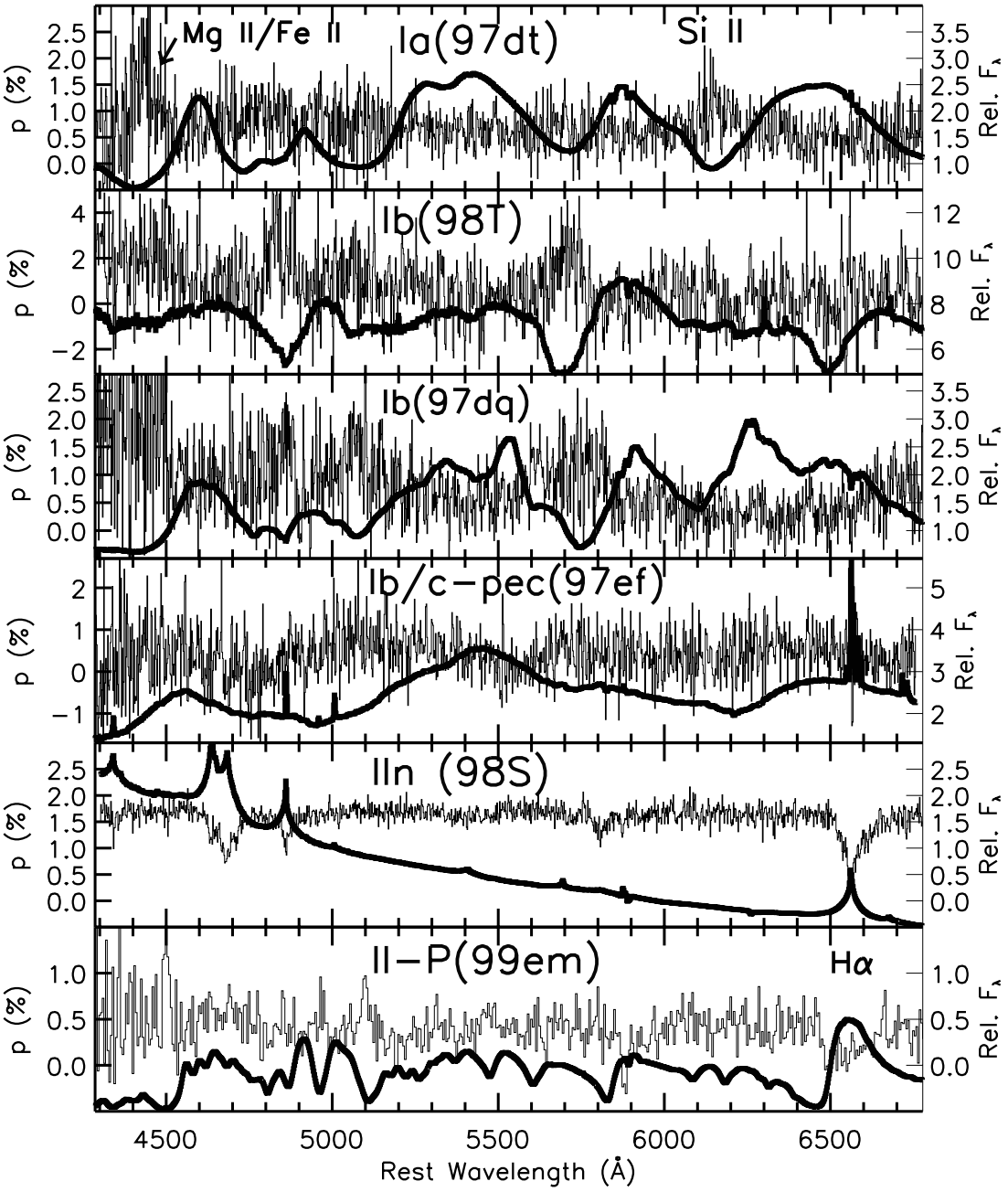
Mg II/Fe II
Ia(97dt)
Si II
Ib(98T)
Ib(97dq)
Ib/c−pec(97ef)
IIn (98S)
II−P(99em)
Hα
p (%)
Rel. F_λ
Rest Wavelength (Å)
4500
5000
5500
6000
6500

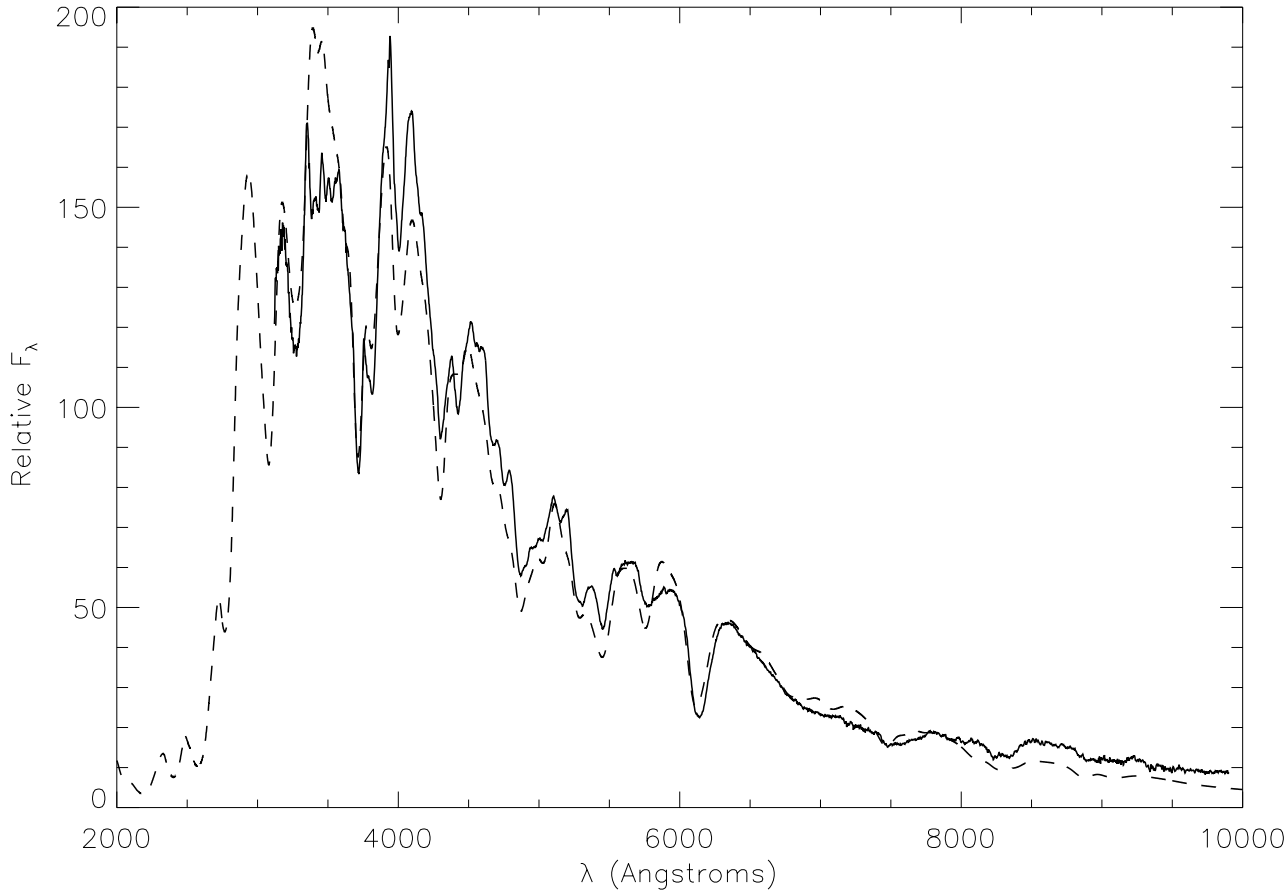
200
150
100
50
0
Relative F_λ
2000
4000
6000
8000
10000
λ (Angstroms)